Theoretical Investigation of Soot Nanoparticle Inception via Polycyclic Aromatic Hydrocarbon Coagulation (Condensation): Energetic, Structural, and Electronic Features

UNIVERSITÀ DEGLI STUDI DI TORINO

Theoretical investigation of soot nanoparticle inception via PAH coagulation (condensation). Energetic, structural, and electronic features.

Anna Giordana, Andrea Maranzana, and Glauco Tonachini*

Dipartimento di Chimica Generale e Chimica Organica, Università di Torino,
Corso Massimo D'Azeglio 48, I-10125 Torino, Italy

Abstract. Carbon nanoparticles, generated during combustion at relatively low [O_2], or under pyrolysis conditions, can be seen both as soot precursors and as primary pollutants in themselves, since they are also directly emitted in the troposphere by vehicles. Soot particle inception (transition of relatively low-mass molecular systems from the gaseous phase to a solid nature) occurs at least in part via polycyclic aromatic hydrocabon (PAH) coagulation/condensation. Complexes of different PAH systems, bound only by dispersion /multipolar forces, are investigated here by density functional theory, and their structural and energetic features discussed. The energetic features of the complexes allow to define an inter-plane interaction energy per C atom which compares satisfactorily with published experimental data on graphite exfoliation (i.e. removal of a single layer from the top of its bulk). The temperature dependence of the equilibrium K for these systems is then calculated, to estimate the importance of PAH coagulation (condensation) in carbon nanoparticle generation. Energy alone would suggest that the larger interacting systems will be better stabilized by dispersion forces, but the trends in free energies are affected also by the entropy factor. This implies that beyond some temperatures the components of the largest systems will be more prone to fly apart than those of smaller systems, thus limiting the size of crystallites beyond some temperature. On the basis of our computational results, at high temperature sheer stacking via van der Waals interaction can hardly be a major factor in causing soot nanoparticle inception.

Keywords:

1) coagulation; 2) carbon nanoparticles; 3) ultrafine particulate; 4) PAH; 5) density functional theory.

---

* e-mail: glauco.tonachini@unito.it - phone: ++39-011-6707648 - fax: ++39-011-2367648

Introduction

Coagulation of gas phase PAH (or PAH-like) systems, interacting through dispersion and multipolar forces, can start the formation of crystallites in nascent soot nanoparticles: its importance as a function of temperature is investigated here by Density Functional Theory.

Carbonaceous particulate is a significant contributor to the overall mass of atmospheric aerosol.[1] It is known that soot particles have a variable nature, depending on several parameters, as fuel, temperature, kind of flame, use of an engine, and so on.[2,3] Based on the properties their exhibit under particular experimental circumstances, further distinct-ions between elementary carbon (EC), black carbon (BC), or soot carbon are sometimes introduced.[3,4] Their structure can be more or less disordered, but when they present more ordered zones (crystallites), these are graphenic in nature, turbostratic, and can be seen as stacks of PAH-like units.[5,6,7,8] The particle's nanostructure depends upon synthesis conditions, and can be in part amorphous, in part made by cristallites.[2] These are made by graphenic layers (platelets, or lamellae), which can be curved and present defects. The approximately spherical aggregates further group as chain clusters of different shapes.[9]

PAHs not only share the same nature and origin of soot platelets (the same combustion processes at relatively low O_2 concentrations[10,11] or pyrolysis)[12] but can also be found associated with soot.[13,14] Both are of concern as regards human health, since, in part-icular, ultra-fine soot aerosol can carry PAHs and derivatives deeply into the respiratory apparatus. On the other hand, since technological applications have been imagined, the synthesis and study of very large systems has appeared promising.[15] Moreover, both soot and PAHs have been tentatively identified also in the interstellar medium, in the envelopes of carbon-rich stars, and in planetary atmospheres.[16]

PAHs are often considered as soot precursors,[17] but other opinions have been put forth.[18] Homann put forward that the reactions leading to PAHs could also bring about the formation of more

irregular structures, called "aromers", starting from association between PAHs and subsequent H_2 losses (ref. 10, pp 2448-2450). These intermediate struct-ures could grow as cages with a higher or lower H content, and get some curvature. They could be seen as candidate precursors of fullerenes and soot both, as a function of temp-erature, and depending on the relative abundance of small growth components, as HCCH.

Soot formation has been reviewed recently.[19] Ultra-fine molecular particles, whose size is 1.5-4 nm, have a likely role as precursors of carbonaceous particulate. They have been identified under different conditions and by way of different techniques, as photoionization mass spectrometry (PI MS), small-angle X-ray scattering (SAXS), laser induced fluorescence (LIF), Laser Induced Incandescence (LII), and UV measurements. In addition to being soot precursors, these ultrafine particles can be emitted directly from combustion engines into the environment. The generation modes of these precursors, which present a transition from the gaseous phase to a solid nature, is in part to be clarified.[20,21] They can exist both under sooting or non-sooting conditions, and coexist with particles whose dimensions exceed 10 nm, generated by coagulation or condensation (bimodal nature).[22] A possible distinction of soot precursor molecules vs particles has been based on the use of PI MS.[23,22,24,25] There, mode A (m/z peaking around 2500 u, with diameter d ≈ 1.8 nm) was identified as PAH clusters bound by aliphatic bridges, while mode B (a broader distribution with m/z around 17000 u, with diameter d ≈ 3.3 nm) was attributed to PAH stacks.

In recent times, a study carried out by the SAXS technique in an ethene-air diffusion flame, provided a detailed and interesting description of the situation at different heights-above-burner (z).[26] The Authors observed, at very low z (≈ 3 mm), a single mode (particle size ≈ 4-6 nm), corresponding to “sub-primary” particles, which then evolves to bimodal for z > 5 mm. At intermediate z values ($z \approx 9 - 15$ mm), two peaks corresponding to sizes of 4 and 12 nm are thus detected, and a depletion of the sub-primary peak in favour of the the primary particles mode (10-12 nm) was concurrently observed. Consequently, a single mode was

found again when proceeding to $z \approx 20$ mm (size > 12 nm). Furthermore, the presence of very small nuclei (1.5 – 2 nm) was detected, which have a nucleation burst at $z \approx 3$ mm and gradually desappear proceeding towards $z \approx 20$ mm. Therefore, three different size modes for soot nanoparticles have been identified.

The particle inception problem can be tackled by studying it at different scales and by different theoretical tools.[27] In 2008, Herdman and Miller have tuned intermolecular potentials to study the formation of this kind of clusters.[28] They found that the binding energies so determined for dimers rise with molecular size, approaching asymptotically, as values per carbon atom, the *exfoliation* energy of graphite, i.e. removal of a single layer from the top of its bulk.[29] This quantity had been experimentally assessed by Zacharia, Ulbricht, and Hertel as ca. 1.2 kcal mol^{-1} per carbon atom.[30] On examining piles of different size, Herdman and Miller also found that other limits were approached, scaling linearly with the molecular mass of the monomer. Their conclusions are that the estimated binding energies are large enough to allow the existence of such stacks at flame temperatures for the majority of PAHs falling along the Sein-Fahr *stabilomer* grid.[31] To a similar conclusion came Schuetz and Frenklack, who carried out molecular dynamics calculations on two colliding pyrene molecules, and concluded that the energy transfer to internal rotational motions that takes place upon collision is effective in stabilizing pyrene dimers.[32] This would occur to a point that they can survive flame conditions long enough to evolve into soot nuclei. A very recent review by Hai Wang discusses these and other aspects of soot inception.[33]

In this study, we model the initial nucleation steps by quantum mechanical methods, applied to molecular systems, limiting the study to the process of coagulation. The growth of an aromatic system adsorbed on a model soot platelet has been studied recently,[34] while nucleation by chemical bond formations will be the subject of a follow up paper. The very first growth steps of systems made by PAH units, taking place through van der Waals associations, hint to the transition from complex (but still rather low-molecular-weight) systems, toward very small solid state particles. However, a rigorous definition of this transition (apart from the proposal based on PI MS results mentioned above) does not appear to be

available.[11] Thus, the initial particle growth is described here as coagulation taking place through associaton of R to P, both PAHs, to produce R : P, or associaton of R to P:Q to produce R : P:Q. These steps involve in the first case R : P systems up to 296 C atoms, whose dimensions are at most ca. 2.4 nm, in the second case stacks containing at most 200 C atoms, whose dimensions are ca. 6.17 nm (stack height, twice the approximate “interlayer” distance for three layers) and 1.7 x 1.6 nm lateral dimensions. The role of temperature in defining the equilibrium constant K(T) for $R + P \rightleftarrows R{:}P$ is then assessed.

The choice of the models chosen to simulate the adsorption onto a particle is based on the following considerations. The size of the mentioned soot platelets or lamellae is finite, and sometimes not very large, while stacks can also be present when the nascent soot particles begin to grow (nucleation). For instance, the following features have been reported: the presence of "initial layers planes composed of about 10-ring benzenoids",[5] or stacks tipically made by 3-4 layers, each layer having "in-plane dimensions of several Ångstroms",[6] or graphitic crystallites ~2-3 nm in size, distributed in an amorphous matrix,[7] or crystallites whose lateral size is ca. 2 nm, and thickness of about 3 carbon layers (i.e. 1 nm).[8] Precursor PAHs and nanoparticles can on the other hand coexist with larger aggregates, and contribute to the presence of an outer layer of adsorbed PAH molecules on the aggregates themselves.[35] All this considered, it seems appropriate to simulate PAH coagulation through molecular calculations on a series of PAHs. Since also PAH condensation onto a pre-existing soot platelet or crystallite should be a quite similar process [11] we will proceed by modeling also the adsorbant surface by a PAH molecule.

Theoretical Method

Stationary points on the energy hypersurface were determined by gradient procedures[36] within the Density Functional Theory (DFT),[37] and making use of the M06-2X functional.[38] The M06-2X functional has been designed to allow the study of complexes of the van der Waals type, in which dispersion forces play a significant or dominant role. For this study in particular, it allows to define the interaction energies of graphenic (PAH) model systems. It is appropriate to mention that a special issue of Phys Chem Chem Phys, dedicated to the subject *Stacking Interactions*, has appeared recently.[39]

The basis set flexibility was forcedly limited here by the size of the systems studied. So, the polarized split-valence shell 3-21G(d) basis set[40] was used in the DFT optimizat-ions and subsequent vibrational analyses and thermochemistry assessments (which however resulted unsfeasible for the largest systems). Whenever distinct moieties interact, the Basis Set Superposition Error (BSSE) relevant to their interaction is accounted for by the counterpoise (CP) method, thus providing the CP-corrected energy differences reported thoughout the paper.[41] The thermochemical corrections, applied when possible, gave estimates of the zero point vibrational energy, by which the relative energies were corrected (ΔE_{ZPE}), and allowed to estimate relative enthalpies (ΔH) and Gibbs free energies (ΔG). The thermochemistry was assessed in all cases at temperatures ranging from room T up to those typical of combustion. Energetics is reported in kcal mol^{-1} and temperatures in Kelvin degrees throughout the paper.

We have initially tested the performances of M06-2X, when used with the modest 3-21G(d) basis set,[42] for the case of the benzene dimer, for which an experimental datum is available. The procedure just outlined yields for benzene (CP-corrected) ΔE_{ZPE} = –0.85 kcal mol^{-1}, that underestimates the experimental values of –1.6 $\pm$ 0.2 kcal mol^{-1}[43] or even 2.4 $\pm$ 0.2 kcal mol^{-1}.[44,45] A better result is obtained for naphthalene, where we get ΔE_{ZPE} = –2.95 kcal mol^{-1}, in (a probably fortuitous optimum) agreement with the experimental D_0 assessment of –2.88 kcal mol^{-1}. [46]

All calculations were carried out by using the GAUSSIAN 09 system of programs.[47] The MOLDEN program was exploited for the graphics.[48]

Results and discussion

Van der Waals complexes of different PAH systems R : P between a smaller R positioned approximately in the middle of a larger P, are considered initially. The two molecules have a parallel displaced arrangement (a π system facing another π system with non-eclipsed C atoms) and interact attractively mainly via “interlayer” dispersion forces.[49] The relevant energetics (defined as detailed here below) is reported in **Tables 1** and **2**. Data pertinent to R : P: Q stacks are in **Table 3** and **Table 4**. Below, the ΔE suffix indicates the nature of the PAH association whose energetics is appraised (the association on which attention is focused is indicated by a colon: $\Delta E_{R:P}$, $\Delta E_{R:PQ}$, $\Delta E_{RP:Q}$, or $\Delta E_{R:P:Q}$).

Different PAH clusters are studied to assess the following points.

(1) On the basis of the $\Delta E_{R:P}$ estimates, which vary for each R as a function of P's increasing size, we attempt to define a limit for each R, $\Delta E_{R:P}(R)$.

(2) A value "per C atom", $\Delta E_C(R)$, is provided by $\Delta E_{R:P}(R)$, directly divided by the number of carbons contained in R. Then, excluding the largest R systems, a limiting value ΔE_C can be defined for the series of $\Delta E_C(R)$ values, as R increases its size. The relevant enthalpy difference ΔH_C (computed when feasible) can then be compared with the experimental activation energy per C atom for graphite exfoliation, seen as an asymptotic limit.

(3) The extent of the change in interaction energy $\Delta E_{R:P}$ upon moving R off the central zone of P towards its border is then appraised for a limited set of R : P associations.

(4) Then, calculations on stacks built from three PAH components (R, P, and Q) allows to assess (a) how the two-component interaction energies $\Delta E_{R:P}$ are altered by the presence of a third sheet Q (by

defining $\Delta E_{R:PQ}$), and (b) the stretching energy, i.e. the complete separation of the three components, as $\Delta E_{R:P:Q}$.

Points 1-4 will be dealt with in § 3.1.

(5) Finally, in § 3.2, the temperature dependence of the thermodinamic constant K for the equilibrium R + P ⇄ R:P is assessed, to estimate the importance of coagulation (or condensation) in carbon nanoparticle generation. Also the temperature dependence of K for the R + P + Q ⇄ R:P:Q equilibrium is studied, but only in the case "R = P = Q = coronene". Some brief considerations on the possibility of predicting the occurrence of two-term associations, as nuclei precursors, are then offered in § 3.3. A final comment on structural features is presented in § 3.4.

3.1 Assessment of the stacking energy. We have first carried out some series of calcul-ations, to assess how the interaction energy $\Delta E_{R:P}$ varies in the R : P complexes. In these, R are: benzene (R6 for short), coronene (R24), and ovalene (R32); a few additional computat-ions involve the larger PAHs R42 and R80. All of these Rn are adsorbed on a series of PAHs P, which are larger then them, to different extents, but in any case large enough to "surround" the whole R, hydrogens included, by an extra loop of hexagonal ring (border-ing). One exception is R80:P96. It comes out that the best arrangement is in general the parallel displaced one mentioned above.

(1) A first purpose is to assess, for each R, how rapidly the association energy estimate, as a function of P's increasing size, can proceed toward a limiting value $\Delta E_{R:P}(R)$. See the A, B, C columns in **Table 1** (values are reported with two decimal places to allow an easier appraisal of the variations). In the case of R6, bordering the initial P by a complete series of hexagonal rings has some effect δ on the estimate of the adsorption $\Delta E_{R:P}$ (from A to B: δ_{AB}= -0.5 kcal mol^{-1}), but convergence toward a limiting value $\Delta E_{R:P}(R)$ is apparently rather fast (from B to C: δ_{BC} = -0.1 kcal mol^{-1}). For R24, δ_{AB} = -1.1, then δ_{BC} = -0.2 kcal mol^{-1}. Similarly for for R32, δ_{AB} = -1.4, then δ_{BC} = -0.2 kcal mol^{-1}. Consequently, we can assume that the final value (C) is a sufficiently good estimate of $\Delta E_{R:P}(R)$. Apparently, if the extent of the dispersion interaction increases as

the area involved (approximately defined by the size of R), the bordering effect mainly involves the interaction of the perimeter C–H bonds of R with the underlying P and can be expected to grow up as the perimeter itself and up to a point. These traits encourage to extend the study on one hand to larger R systems, keeping P's size generally larger than R by one extra ring of hexagons. On the other hand, the size of both R and P is kept rather limited, for obvious practical reasons, but also keeping in mind the available data on the observed dimensions of crystallites.[5-8]

Table 1. Computed $\Delta E_{R:P}$ estimates of the "adsorption" energy[a] of R onto P and the corresponding values per carbon atom, ΔE_C.[b]

Rn	"adsorbed" on Pm A B C	A ΔE ΔE_{ZPE}	B ΔE ΔE_{ZPE}	C ΔE ΔE_{ZPE}
R6	P42, P80, P130	-7.03 **-6.28**	-7.49 **-6.66**	-7.59 **-6.58**
	ΔE_C and $\Delta E_{ZPE,C}$:	*-1.17* ***-1.05***	*-1.25* ***-1.12***	*-1.27* ***-1.10***
R24	P80, P130, P192	-28.93 **-26.29**	-29.97 **-27.02**	-30.16 –
	ΔE_C and $\Delta E_{ZPE,C}$:	*-1.20* ***-1.10***	*-1.25* ***-1.13***	*-1.26* –
R32	P96, P150, P216	-38.68 **-37.40**	-39.44 **-37.53**	-39.62 –
	ΔE_C and $\Delta E_{ZPE,C}$:	*-1.21* ***-1.17***	*-1.23* ***-1.17***	*-1.24* –
R42	P96, P150 –	-49.34 **-47.80**	-51.38 –	
	ΔE_C and $\Delta E_{ZPE,C}$:	*-1.17* ***-1.14***	*-1.22* –	
R80[c]	P150, P216 –	-94.39 –	-97.51 –	
	ΔE_C:	*-1.18* –	*-1.22* –	

[a] units: kcal mol^{-1}. DFT(M06-2X)/3-21G(d) energy differences between optimized R:P structures, and separated R and P moieties, followed by ΔE_{ZPE} [=Δ(E+ZPE)] values, in bold. A, B, C define, for each R, three Pm molecules of different sizes, as specified in the second column. The values in column C can be taken as close approximations to the $\Delta E_{R:P}$(R) limiting values.

[b] values in italic; obtained dividing by n (from Rn), from both plain energies and ZPE-corrected energies.

[c] additional data for R80:P96 (used below for comparative purposes) stand alone, since, in this case only, no bordering of R by P is present: ΔE=-79.89 and ΔE_{ZPE}=-**76.61**. With this R size, we come

to van der Waals interactions close to the strength of a single carbon-carbon bond, ca. 83 kcal mol^{-1}.

(2) $\Delta E_{R:P}$(R), directly divided by the number of carbons contained in R, provides a value "per C atom", ΔE_C(R). One can consider that the most important part of the interaction comes from those parts of the two molecules that are directly superimposed, so that this major component of interaction can approximately be seen as "perpendicular" to the (approximate) molecular planes. At the same time, bordering produces smaller "diagonal" interactions. As an example, if the smaller PAH_1 (see the sketch below) has n_1 carbon atoms, the same number of carbons in the underlying PAH_2 can be assumed to be interested in the "perpendicular" interactions, symbolized in the sketch by some dashed segments. Hence the ΔE_C values are approximately defined by dividing the interaction energy by the number of carbons contained in the smaller PAH.

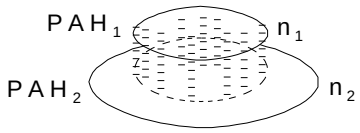

van der Waals
2-term complex

$-\Delta E_C$ values range, in the presence of bordering, from 1.17 (A) to 1.27 (C) kcal mol^{-1}, as the size of the system increases (R6, **Table 1**). This A-C range is slightly reduced for R24 and R32, and for R80 we have 1.18-1.22, but only for A and B. In the only case where bordering is not present (R80:P96), a lower value is obtained, 1.0 kcal mol^{-1}. Up to some system's size, vibrational analysis could be carried out to provide ZPE and thermal corrections. $-\Delta E_{ZPE}$ per C atom ($\Delta E_{ZPE,C}$) values are constantly lower, and span the 1.05-1.17 kcal mol^{-1} range of values. In these cases, enthalpy values can also be obtained from the previously discussed energy values, in order to get an enthalpy value per C atom, ΔH_C. In **Table 2**, the enthalpy differences reported are those obtained for the largest underlying P system in correspondence of which vibrational analysis resulted feasible (C for R6, but only B for R24 and R32). The ΔH values reported are built from energies plus thermal corrections evaluated at the peak temperatures indicated in ref. 30.

Table 2. Computed "adsorption" enthalpies and comparison with the experimental graphite exfoliation activation energy per C atom.[a]

Rn "adsorbed" on Pm		ΔH[b]	ΔH_C[c]	$E_{a,C}$
R6	P130	-6.66	*-1.11*	
R24	P130	-27.30	*-1.14*	1.2 ±0.1
R32	P150	-37.38	*-1.17*	

[a] units: kcal mol^{-1}.

[b] ΔH are interaction enthalpies, from the DFT(M06-2X)/3-21G(d) energy differences obtained for the largest underlying P system in correspondence of which vibrational analysis resulted feasible (B for R24 and R32, C for R6), plus thermal correction at the peak temperatures indicated in ref. 30 (R6: T=151 K; R24: T=390 K; R32: T=490 K).

[c] ΔH_C are the values per C atom, i.e. the computed ΔH divided by the number of C atoms in R (values in italic). They can be compared with the experimental value $E_{a,C}$ for graphite exfoliation, taken from ref. 30.

The ZPE-corrected energy differences and the original energy differences show a regular relative dependence (a linear relationship with r^2=0.9994 and angular coefficient a=0.9688), in such a way that the latter alone can be deemed still apt to provide sufficiently reliable indications for the largest systems, when the vibrational analysis resulted unfeasible.

ΔH_C values can be compared with the *activation energy* $E_{a,C}$ = 1.2 ± 0.1 kcal mol^{-1} determined by thermal desorption spectroscopy and identified with the *interlayer cohesive energy* of graphite.[30] Also an *energy* value of 1.2_7 kcal mol^{-1} (55 meV) based on ab initio Quantum Force Field can be taken into account.[50] Other experimental estimates set ΔE_c (energy, per atom, required to separate graphite into planes at infinite distance apart, i.e. the *stretching* energy) in the range 1.1_5-1.3_8 kcal mol^{-1} (50-60 meV), as discussed in a computational study on interlayer binding in graphite[51]. Previous experimental estimates set the *exfoliation* energy at 0.99 ± 0.1 kcal mol^{-1},[52] or even down to ca. 0.81 kcal mol^{-1} (mentioned as *cohesive energy* of graphite). These assessments present some uncertainties discussed in ref. 30. Two studies on desorption of a variety of PAHs from a soot surface have also appeared very recently.[53,54]

(3) Moving R toward the border shows that the variation in $\Delta E_{R:P}$ is not very large. For instance: for R6 on P42, $\Delta E_{R:P}$ drops from -7.0 kcal mol^{-1} to -6.2; for R24 on P80, from -28.9 to -26.9; for R32 on P96, from -38.8 to –35.7. The effect is not unexpectedly opposite to what already seen for bordering (loss of "diagonal" interactions).

(4) We have also carried out some calculations on stacks built from three PAH components (one is shown in **Figure 1**). Three layers allow us to determine both exfoliation and stretching energies. For these systems, only plain energy data have been obtained. The estimate of the interaction energy $\Delta E_{R:PQ}$ or $\Delta E_{RP:Q}$ (exfoliation, in which case only one component is separated by the remaining two-term complex) or $\Delta E_{R:P:Q}$ (stretching, with full separation of all overlaid three components) varies in the R:P:Q complexes as shown in **Table 3**. The second column of data reports the relevant R:P two-layer values for sake of comparison. The obtained exfoliation energies are close to those obtained for two-layer stacks, $\Delta E_{R:P}$. Yet, they show a moderate lowering, that might suggest a reduced interaction between stack components as the number of layers increases.

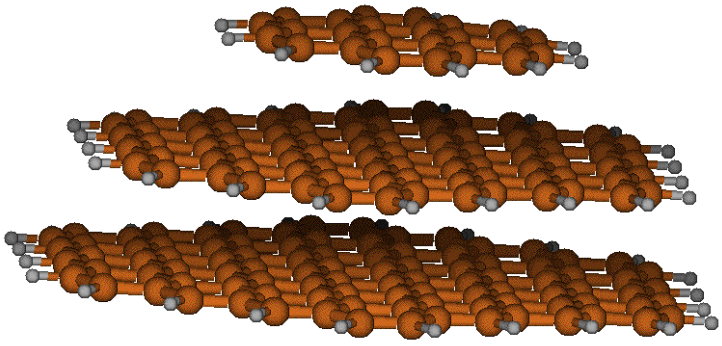

FIGURE 1. The R24:P80:Q96 stack.

If the stack is composed by three overlaid PAHs of increasing size (see the sketch below), the same argument used to introduce ΔE_C for a two-term complex would suggest that the major component of the PAH_2-PAH_3 interaction is related to that part of PAH_3 "shadowed" by the smaller PAH_2 carbons (in number of n_2). As done above, this is symbolized in the sketch by some thicker dashed segments. The PAH_1-PAH_2 perpendicular interaction is represented by thinner dashed segment. In this case the ΔE_C values could be

approximately defined by dividing the stretching interaction energy by the sum of the number of carbons contained in the smaller PAHs ($n_1 + n_2$).

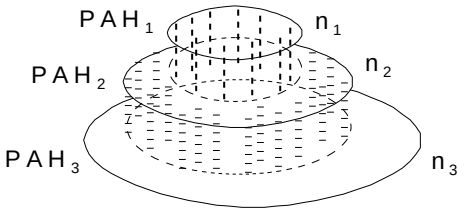

3-term stack

Table 3. Computed exfoliation energies[a] for three-layer stacks R:P:Q.

R:P:Q[b]	$\Delta E_{R:PQ}$ or $\Delta E_{RP:Q}$	$\Delta E_{R:P}$
R6 from P42:Q80	-6.80	-7.03
ΔE_C:	-1.13	-1.17
R24 from P80:Q96	-28.05	-28.93
ΔE_C:	-1.17	-1.20
R24:P80 from Q96[c]	-79.01	-79.89
ΔE_C:	-0.99	-1.00
R24 from P24:Q24 [c]	-14.12	-15.32
ΔE_C:	(-0.59)[d] -1.01[e]	(-0.64)[d] -1.09[e]

[a] units: kcal mol^{-1}.

[b] DFT(M06-2X)/3-21G(d) energy differences between optimized R:P:Q structures, and separated R and P:Q (or R:P and Q, third case) moieties, where P and Q (or R and P, third case) are still interacting. The values per C atom are reported just below them in italic (initial values divided by 6, 24, and 80).

[c] These data compare with those for R80:P96. For R80 and P96, no bordering of the smaller moiety by the larger is present, so that they can be seen as standing alone. No bordering is present also in R24:P24.

[d] In this case the coronene molecules slip aside one with respect to the other, in such a way that some carbons on the perimeter of one molecule have a projection out of the perimeter of the next molecule. Hence dividing by 24 results in an underestimation of ΔE_C (figures in parenthesis).

[e] To obtain a more correct estimate we have excluded the carbon whose projection falls out of the underliyng PAH (-14.12 and -15.32 are consequently divided by 14).

In a more general form, this number could be defined as the sum of all carbons of one PAH whose projection falls within the perimeter of the underlying PAH. Diagonal interactions are taken into account, but this protocol avoids counting some perpendicular and diagonal interactions more than once.

An additional test involved the dimer and the trimer of coronene. The energy data are reported in **Table 4**.

Table 4. Computed stretching energies[a] for three-layer stacks R:P:Q.

R:P:Q[b]	$\Delta E_{R:P:Q}$
R6:P42:Q96	-56.14
ΔE_C:	-1.17
R24:P80:Q96[c]	-107.94
ΔE_C:	-1.04
R24:P24:Q24 [c]	-29.45
ΔE_C:	(-0.61)[d] -0.89[e]

[a] units: kcal mol^{-1}.

[b] DFT(M06-2X)/3-21G(d) energy differences between optimized R:P:Q structures, and completely separated R, P, and Q molecules.

[c] These data compare with those for R80:P96. For R80 and P96, no bordering of the smaller moiety by the larger is present. The same trait is present also in R24:P24:Q24.

[d] In this case the stack comes out to have significantly displaced components, hence dividing by 48 results in an underestimation of ΔE_C (figures in parenthesis).

[e] To obtain a more correct estimate we have excluded the carbon whose projection falls out of the underliyng PAH (-29.45 is consequently divided by 33).

This kind of calculation was run with the purpose of carrying out the vibrational analysis, hence to assess the temperature dependence of the stretching free energy, dealt with in the following subsection. Since the coronene molecules slip aside one with respect to the other (sketch below), some carbons on the perimeter of one molecule have a projection out of the perimeter of the next molecule (arrows) thus reducing the perpendicular interactions, symbolized again by some dashed segments. We relied on the protocol just discussed to estimate the ΔE_C value.

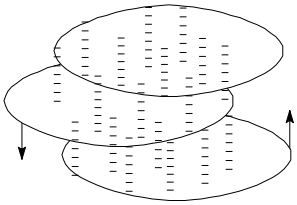

R24:P24:Q24
coronene$_3$ stack

3.2 T dependence of stacking. As the size of a π system grows, van der Waals interactions (mainly dispersion forces in the case of stacking) will be more and more effective in favoring the piling up of approximately planar molecules. Through this process, coagul-ation will take place (it can also be seen as condensation, depending on how the larger system P is identified, since a clearcut border cannot be defined). Sticking can be expected to be temperature dependent, and to take place in any case more easily at lower temperatures. We can suppose that equilibrium can be attained, though it is not to be taken for granted. Inspection of **Figure 2**, where the estimates of the K(T)=exp(-ΔG/RT) for the equilibrium R + P $\rightleftarrows$ R:P are displayed as -Log K(T), shows that each of the three curves exhibit the expected preference for lower temperatures (larger K values). K is expressed assuming a standard state of 1 molecule cm^{-3}. Then, it can be observed that the larger the adsorbed aromatic, the more pronounced is this preference: a steeper curve indicates that R32 is the most sensitive, a flatter one that R6 is the less. So, the relative behavior of the leftmost part of the curves is intuitively expected on the basis of an energy factor alone, when

considering that dispersion forces will be more effective when larger systems are involved. However, though one might anticipate that the interaction will be favored by an increasing size of the interacting moieties at any T (on the basis of cumulative dispersion forces), the curve crossings show that this is not the case.

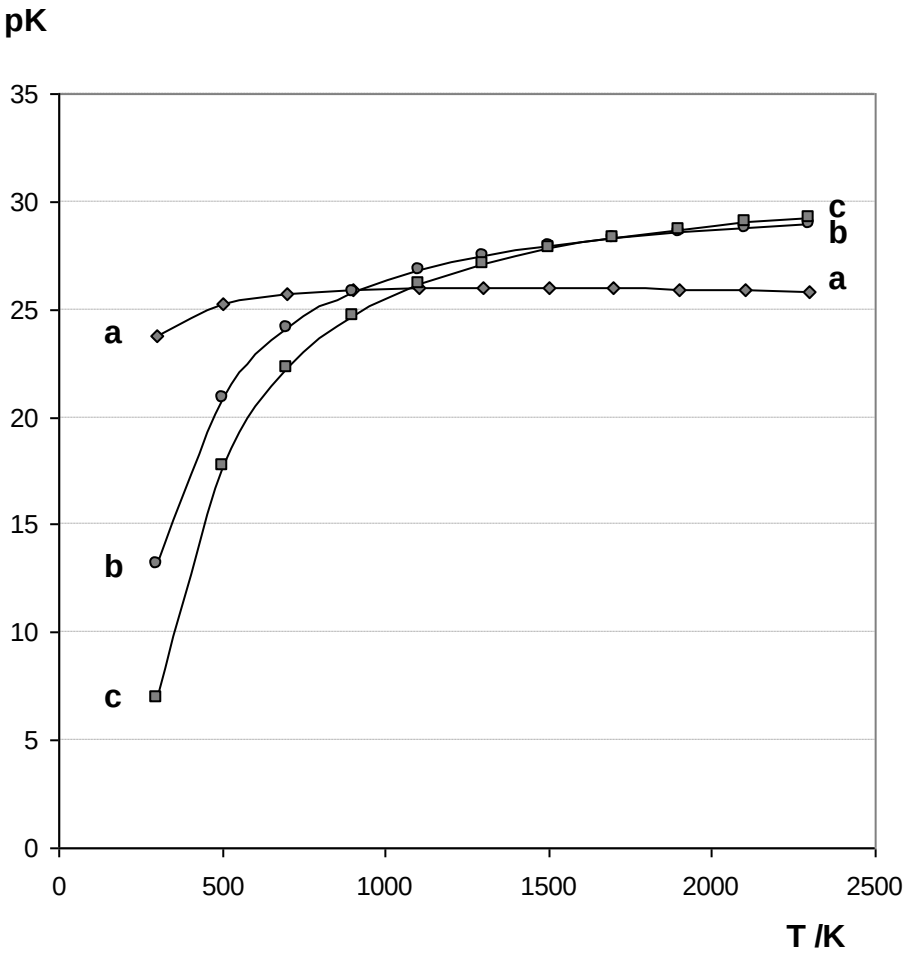

FIGURE 2. -Log K (T) for the equilibrium R + P ⇄ R:P. Curve a, diamonds: benzene, R6. Curve b, circles: coronene, R24. Curve c, squares: ovalene, R32.

This additional and interesting feature is due to the contribution of the -TΔS term in ΔG, whose importance obviously grows up with T, and determines this feature, close to 1000 K for R6-R24, and around 1500 K for R24-R32. An interesting consequence of these crossings is that they will apparently tend to limit the dimensions of crystallites possibly formed at higher temperatures.[32] As regards temperature, soot inception is indicated in a recent book to occur in the approximate temperature range 1300-1900 K, on the

basis of a collection of results obtained by various researchers.[55]

3.3 Presence of two-term PAH associations in flames. As **Figure 2** shows, in the 1000-2000 K temperature range, stacks can survive in relatively small molar fractions. By using experimental data on PAH concentration in flames, an indeed very approximate quantification of two-term associations R:P presence can be attempted as follows, and compared to our K estimates. At T = 1500 K, for instance (see, for this choice, the flame temperature reported in Fig. 2 of ref. 56), a number of molecules of ca. 5×10^{18} will be present in 1 cm^3, if P = 1 atm. The molar fraction of all PAHs present in a benzene flame (x_{PAH}) was recently reported to range approximately from 4 to 2×10^{-4}, depending on z (Fig. 4 in ref. 56) corresponding to ca. 10^{15} molecules per cm^3 (equivalent to [R] or [P]). By having $K = [R:P] / [R]\,[P]) \approx 10^{-26}$, we get a rough estimate of the concentration of these small "nuclei precursors", $[R:P] \approx 10^4$ molecules cm^{-3}.

3.4 Structural effects of stacking. If the stacked moieties are not identical, we find that some curvature in the larger PAH (P) can be induced by the smaller (R). This is illustrated by the complex between R32 and P96 (**Figure 3**). It can be seen that P becomes to some extent concave toward R. This could be a cumulative effect due to the sum of minute attractions among the C–H small dipoles present all around R and the π system of P's outer ring of carbon hexagons. The overall effect does not necessitate to be large. In fact, one can assess the deformation energy of P alone, by subtracting the energy of P's optimized structure from that corresponding to P's curved structure in the complex. This deformation energy E_D is small and provides a lower limit estimate to the stabilization attained in the complex when P departs from a planar geometry. For instance: E_D = 0.31 kcal mol^{-1} for P130 in R6:P130; E_D = 0.76 kcal mol^{-1} for P192 in R24:P192; E_D = 1.47 kcal mol^{-1} for P126 in R32:P126). These values provide (non unexpectedly) the picture of PAHs as quite flexible objects.[57] They can be seen as able to adapt their shape to some extent to match the surface situation of an underlying nucleus to which they are getting adsorbed.[58,59] In turn, this effect could be in part at the origin of the

curved aspect of larger aggregates (other contributions could come from defects, or presence of non-6-membered rings).

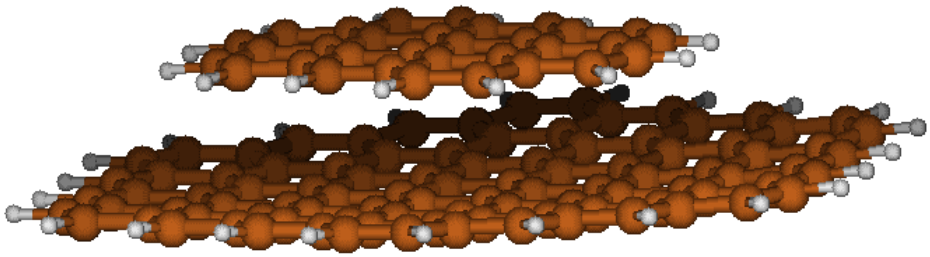

FIGURE 3. Complex between R32 (ovalene) and P96.

To put to the test the above hypothesis (C–H dipoles interacting with the closest polarizable π rings), we have run a calculation on a smaller system (ethyne-pentacene). Ethyne has local dipoles associated to its C–H bonds larger that those present in PAHs, due to the sp hybridation of its carbons,[60] and pentacene is presumably even more flexible than the PAHs studied here, which extend in two directions. Moreover, by running this test, we can also assess is if P curvature is an artifact of the very modest basis set we are forced to use with the larger systems. In fact, the limited size of the ethyne-pentacene complex allowed us to run optimizations with an extended basis set, cc-pVQZ (see note 42).

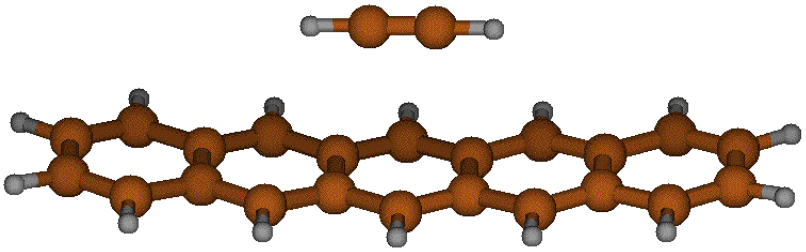

FIGURE 4. Complex between ethyne and pentacene.

Figure 4 conveys a qualitative information about the extent to which pentacene gets curved at the M06-2X/cc-pVQZ level**.** Just to give an idea, we can define the angle α = ∠XMX, defined by the collinear midpoints X of the leftmost and rightmost CC bonds and the center of the central hexagon, M. Its deviation from 180° (α=174.8°) is eligible as an approximate measure of pentacene curvature. The conclusion is

that we are not seeing the result of a basis set artifact: curvature comes from the interaction of the two molecules.

Conclusions

The interaction energies of two PAHs of different sizes, R (smaller) and P (larger) are assessed for different sizes of both. This study shows that, for each R, a limiting value for their interaction energies is attained rather soon upon enlargement of P. The limiting value of the interaction enthalpy per C atom, ΔH_C, ranges from 1.11 to 1.17 kcal mol^{-1}, and compares well with an experimental estimate relevant to the exfoliation of graphite (E_a = 1.2 ± 0.1 kcal mol^{-1}).

Then the T-dependence of the stacking thermodinamic constant K for the equilibrium R + P ⇄ R:P is assessed. Though the energy factor alone would suggest that the larger interacting systems will be better stabilized by dispersion forces, the trends in free energies are affected also by the entropy factor, and this induces crossings in the K(T) curves. These crossings mean that beyond some temperatures the components of the largest systems will be more prone to fly apart than those of smaller systems. This feature suggests in turn that the size of crystallites will be limited beyond some temperature by the more pronounced tendency of smaller graphenic units to stay piled together.

The study of some three-membered stacks shows on one hand that the addition of a third sheet hardly affects the exfoliation energy values obtained for the two-membered complexes. On the other hand, the stretching energies per carbon atom in three-term associations result to be not significantly different from the exfoliation energies in the same models.

Acknowledgments. This work was conducted in the frame of EC FP6 NoE ACCENT (Atmospheric Composition Change, the European NeTwork of Excellence). AG is supported by a research bursary by Regione Piemonte.

Supporting Information for this article is available and includes the geometries and energetics of all optimized structures.

REFERENCES

[1] Cooke, W. F.; Wilson, J. J. N. *J. Geophys. Res.* **1996**, 101, 19395-19409; Liousse, C.; Penner, J. E.; Chuang, C.; Walton, J. J.; Eddleman, H.; Cachier, H. *J. Geophys. Res.* **1996**, 101, 19411-19432.

2 Vander Wal, R. L.; Tomasek, A. J. *Comb. Flame* **2004**, 136, 129-140.

3 Currie, L. A.; Kessler, J. D. *Atmos. Chem. Phys. Discuss*. **2005**, 5, 3341-3366.

4 Reisinger, P.; Wonaschutz, A.; Hitzenberger, R.; Petzold, A.; Bauer, H.; Jankowski, N.; Puxbaum, H.; Chi, X.; Maenhaut, W. *Environ. Sci. Technol*. **2008**, 42, 884–889.

5 see for instance: Ishiguro, T.; Suzuki, N.; Fujitani, Y.; Morimoto, H. *Comb. Flame* **1991**, 85, 1-6. See in particular mid p 4.

6 Vander Wal, R. L. *Comb. Sci. Tech.* **1998**, 132, 315-323.

7 Ginzburg, B. M.; Tuĭchiev, Sh.; Tabarov, S. Kh.; Shepelevskii, A. A. *Chrystallography Reports* **2007**, 52, 187-190.

8 Popovitcheva, O. B.; Persiantseva, N.M.; Trukhin, M. E.; Rulev, G. B.; Shonija, N. K.; Buriko, Y. Y.; Starik, A. M.; Demirdjian, B.; Ferry, D.; Suzanne, J. *Phys. Chem. Chem. Phys.* **2000**, 2, 4421-4426 (see in particular mid p 4423).

9 See for instance: Ivleva, N. P.; Messerer, A.; Yang, X.; Niessner, R.; Pöschl, U. *Environ. Sci. Technol*. **2007**, 41, 3702-3707, and: http://www.ws.chemie.tu-muenchen.de/groups/director /projects0/raman-soot/. Műller, J.-O.; Su, D. S.; Jentoft, R. E.; Wild, U.; Schlőgl, R. *Environ. Sci. Technol*., **2006**, 40, 1231-1236.

10 Homann, K.-H. *Angew. Chem. Int. Ed.* **1998**, 37, 2434-2451.

11 Finlayson-Pitts, B. J.; Pitts, J. N., Jr., *Chemistry of the Upper and Lower Atmosphere*; Academic Press, New York, 2000, ch. 10. See, in particular, Figures 10.2 and 10.3; Ch. 9, p. 349; Ch. 9, p. 378.

12 See for instance: Böhm, H.; Jander, H. *Phys. Chem. Chem. Phys.* **1999**, ***1***, 3775-3781. Ledesma, E. B.; Kalish, M. A.; Nelson, P. F.; Wornat, M. J.; Mackie, J. C. *Fuel* **2000**, 79, 1801-1814. Naydenova, I.; Vlasov, P. A.; Warnatz, J. *Proc. Eur. Comb. Meeting* **2005**. Jäger, C.; Huisken, F.; Mutschke, H.; Llamas-Jansa, I.; Henning, Th. *Astrophys. J.* **2009**, 696, 706-712. Jäger, C.; Mutschke, H.; Huisken, F.; Krasnokutski, S.; Staicu, A.; Henning, Th.; Poppitz, W.; Voicu, I. *Astrophys. J. Suppl.* **2006**, 166, 557-566.

13 Pöschl, U.; Letzel, T.; Schauer, C.; Niessner, R. *J. Phys. Chem. A* **2001**, 105, 4029-4041.

14 Kamens, R. M.; Guo, J.; Guo, Z.; McDow, S. R. *Atmos. Environ*. **1990**, 24A, 1161-1173.

15 Simpson, C. D.; Brand, J. D.; Berresheim, A. J.; Przybilla, L.; Räder, H. J.; Müllen, K. *Chem. Eur. J.* **2002**, 8, 1424-1429.

16 Wilson, E. H.; Atreya, S. K. *Planet. Space Sci.* **2003**, 51, 1017-1033. Cherchneff, I.; Barker, J. R.; Tielens, A. G. G. M. *Astrophys. J.* **1991**, 377, 541-552. Allamandola, L. J. ; Tielens, A. G. G. M.; Barker, J. R. *Astrophys. J. Suppl. Series* **1989**, 71, 733-775.

17 Bachmann, M.; Wiese, W.; Homann, K.-H. *Proc. Comb. Inst.* **1996**, 26, 2259-2267.

18 Siegmann, K.; Sattler, K.; Siegmann, H.C. *J. Electron Spectr.* **2002**, 126, 191-202.

19 Xi, J.; Zhong, B.-J. *Chem. Eng. Technol.* **2006**, 29, 665-673.

20 D'Anna, A.; Comodo, M.; Minutolo, P. *Comb. Sci. Tech.* **2008**, 180, 758-766. D'Anna, A.; Commodo, M.; Sirignano, M.; Minatolo, P.; Pagliata, R. *Proc. Comb. Inst.* **2009**, 32, 793-801. D'Anna, A.; D'Alessio, A.; Minutolo, P. (H. Bockhorn ed) Spectroscopic and Chemical Characterization of Soot Inception Processes. *Soot Formation in Combustion* pp. 83-103. Springer-Verlag, Berlin 1994— Premixed Flames at Atmospheric Pressure. Commodo, M.; Violi, S.; D'Anna, A.; D'Alessio, A.; Allouis, C.; Beretta, F.; Minutolo, P. *Comb. Sci. Tech.* **2007**, 179, 387-400. D'Anna, A.; Commodo, M.; Violi, S.; Allouis, C.; Kent, J. *Proc. Comb. Inst.* **2007**, 31, 621-629.

21 Finlayson-Pitts, B. J.; Pitts, J. N., Jr. *Chemistry of the Upper and Lower Atmosphere*; Academic Press, New York, 2000, ch. 9, Sec.2, p. 358.

22 Gonzalez Baquet, T.; Grotheer, H.-H.; Aigner, M. *Rapid Commun. Mass Spectrom.* **2007**, 21, 4060-4064.

23 Happold, J.; Grotheer, H.-H.; Aigner, M. *Rapid Commun. Mass Spectrom.* **2007**, 21, 1247-1254.

24 Zhao, B.; Yang, Z.; Johnston, M. V.; Wang, H. *Proc. Comb. Inst.* **2005**, 30, 1441-1447.

25 D'Anna, A. *Proc. Comb. Inst.* **2009**, 32, 593-613.

26 di Stasio, S.; Mitchell, J. B. A.; LeGarrec, J. L.; Bienner, L.; Wulff, M. *Carbon* **2006**, 44, 1267-1279.

27 See for instance: Chung, S. H.; Violi, A. *Carbon* **2007**, 45, 2400–2410. Balthasar, M.; Kraft, M.; Frenklach, M. *Abstracts of papers of the Am Chem Soc* **2005**, 229 (part 1), U860, Abstract O59 - Fuel. Morgan, N.; Kraft, M.; Balthasar, M.; Wong, D.; Frenklach, M.; Mitchell, P. *Proc. Comb. Inst.* **2007**, 31, 693-700.

28 Herdman, J. D.; Miller, J. H. *J. Phys. Chem. A* **2008**, 112, 6249–6256.

29 For layered systems, as graphite, *exfoliation* is opposed to *stretching*, full separation of all layers, or *cleavage*, splitting the bulk into two blocks (sub-bulks). Making reference to the molecular systems studied in this paper, only the energy relevant to the first two processes can be compared.

30 Zacharia, R.; Ulbricht, H.; Hertel, T. *Phys Rev B* **2004**, 69,155406 1-7. *Cohesive energy* is not to be intended, in this context, as that related to the separation of the solid bulk into independent atoms, but only to separation of the component layers.

31 Stein, S. E.; Fahr, A. *J. Phys. Chem.* **1985,** 89, 3714–3725.

32 Schuetz, C. A.; Frenklach, M. *Proc. Comb. Inst.* **2002**, 29, 2307–2314.

33 H. Wang *Proc. Comb. Inst.* **2010**, xx, xxx–xxx - doi:10.1016/j.proci.2010.09.009.

34 Indarto, A.; Giordana, A.; Ghigo, G.; Maranzana, A.; Tonachini, G. *Phys. Chem. Chem. Phys*. **2010**, 12, 9429–9440.

35 Dobbins, R. A. *Aerosol Sci. Tech.* **2007**, 41, 485-496. See also Fig. 7 in: Sirignano, M.; Sgro, L. A.; D'Anna, A.; Minutolo, P. *Comb. Coll.* **2009**, I-14,1-9 (http://www.combustioninstitute.it/proc/proc2009/data/I/I-14.pdf).

36 Pople, J. A.; Gill, P. M. W.; Johnson, B. G. *Chem. Phys. Lett.* **1992**, 199, 557-560. Schlegel, H. B.; in *Computational Theoretical Organic Chemistry*, ed. I. G. Csizsmadia, R. Daudel, Reidel Publishing Co., Dordrecht, The Netherlands, 1981, pp. 129-159. Schlegel, H. B. *J. Chem. Phys.* **1982**, 77, 3676-3681. Schlegel, H. B.; Binkley, J. S.; Pople, J. A. *J. Chem. Phys.* **1984**, 80, 1976-1981. Schlegel, H. B. *J. Comput. Chem*. **1982**, 3, 214-218.

37 Parr, R. G.; Yang, W. *Density Functional Theory of Atoms and Molecules*, Oxford University Press: New York, 1989, ch. 3.

38 Zhao, Y.; Truhlar, D. G. *Theor. Chem. Acc.* **2008**, 120, 215-41.

39 Hobza, P. editor. *Phys. Chem. Chem. Phys.* **2008**, 10, 2581-2865 (a special issue on *Stacking Interactions*).

40 Binkley, J. S.; Pople, J. A.; Hehre, W. J. *J. Am. Chem. Soc.,* **1980**, ***102***, 939-947. The sp basis set 3-21G was enriched with d functions on all carbons (with gaussian exponent = 1.0), and is referred to as 3-21G(d) in this work.

41 Boys, S. F.; Bernardi, F. *Mol. Phys.* **1970**, 19, 553-566. Simon, S.; Duran, M.; Dannenberg, J. J. *J. Chem. Phys.* **1996**, 105, 11024-11031. Kobko, N.; Dannenberg, J. J. *J. Phys. Chem. A* **2001**, 105, 1944-1950.

42 A calculation run with this functional in conjunction with better basis sets could probably produce more accurate results, but the size of the systems investigated in this work does not allow to proceed beyond 3-21G(d). To give an exemple, we optimized the benzene dimer in its parallel displaced geometry at the M06-2X/cc-pVTZ level [cc-pVTZ basis set: Kendall, R. A.; Dunning, T. H., Jr.; Harrison, R. J. *J. Chem. Phys.* **1992**, 96, 6796-806]. It was followed by cc-pVQZ single point computation [Woon, D. E.; Dunning, T. H., Jr. *J. Chem. Phys.* **1993**, 98, 1358-1371]. A M06-2X/CBS (complete basis set) estimate was then obtained by using the

extrapolation formula put forward in: Halkier, A.; Helgaker, T.; Jørgensen, P.; Klopper, W.; Koch, H.; Olsen, J.; Wilson, A. K. *Chem. Phys. Lett.* **1998**, 286, 243-252. The $(C_6H_6)_2$ stability estimate so obtained, Δ(E+ZPE) = -1.76 kcal mol^{-1}, comes out to be in better agreement with the 1991 experimental assessment of D_0 = -1.6 ± 0.2 kcal mol^{-1} [ref. 43], though not as close to the 1987 assessment of 2.4 ± 0.4 kcal mol^{-1} [ref. 44].

43 Krause, H.; Ernstberger, B.; Neusser, H. J. *Chem. Phys. Lett.* **1991**, 184, 411-417.

44 Grover, J. R.; Walters, E. A.; Hui, E. T. *J. Phys. Chem.* **1987**, 91, 3233-3237.

45 Sinnokrot, M. O.; Sherrill, C. D. *J. Phys. Chem. A* **2006,** 110, 10656-10668. From that high-level study we quote: "The observed convergence of our theoretical data gives us confidence that our best estimates of the binding energies are within a few tenths of 1 kcal mol^{-1} of the true values. The most frequently quoted experimental binding energy, D_0 =1.6 ± 0.2 kcal mol^{-1},[ref. 43] is thus clearly too low. However, the older experimental value of 2.4 ± 0.4 kcal mol^{-1} [ref. 44] is well supported by our data."

46 Fujiwara, T.; Lim, E. C. *J. Phys. Chem. A* **2003**, 107, 4381-4386.

47 Gaussian 09, Revision A.02, Frisch, M. J.; Trucks, G. W.; Schlegel, H. B.; Scuseria, G. E.; Robb, M. A.; Cheeseman, J. R.; Scalmani, G.; Barone, V.; Mennucci, B.; Petersson, G. A.; Nakatsuji, H.; Caricato, M.; Li, X.; Hratchian, H. P.; Izmaylov, A. F.; Bloino, J.; Zheng, G.; Sonnenberg, J. L.; Hada, M.; Ehara, M.; Toyota, K.; Fukuda, R.; Hasegawa, J.; Ishida, M.; Nakajima, T.; Honda, Y.; Kitao, O.; Nakai, H.; Vreven, T.; Montgomery, Jr., J. A.; Peralta, J. E.; Ogliaro, F.; Bearpark, M.; Heyd, J. J.; Brothers, E.; Kudin, K. N.; Staroverov, V. N.; Kobayashi, R.; Normand, J.; Raghavachari, K.; Rendell, A.; Burant, J. C.; Iyengar, S. S.; Tomasi, J.; Cossi, M.; Rega, N.; Millam, N. J.; Klene, M.; Knox, J. E.; Cross, J. B.; Bakken, V.; Adamo, C.; Jaramillo, J.; Gomperts, R.; Stratmann, R. E.; Yazyev, O.; Austin, A. J.; Cammi, R.; Pomelli, C.; Ochterski, J. W.; Martin, R. L.; Morokuma, K.; Zakrzewski, V. G.; Voth, G. A.; Salvador, P.; Dannenberg, J. J.; Dapprich, S.; Daniels, A. D.; Farkas, Ö.; Foresman, J. B.; Ortiz, J. V.; Cioslowski, J.; Fox, D. J. Gaussian, Inc., Wallingford CT, 2009

48 MOLDEN: Schaftenaar, G.; Noordik, J. H. *J. Comput.-Aided Mol. Design* **2000**, 14, 123-134. (http://www.cmbi.ru.nl/molden/molden.html)

49 Compare the situation in graphite, where the interlayer interaction is composed by a repulsive "orbital contribution" and the attractive dispersion forces: Schabel, M. C.; Martins, J. L. *Phys. Rev. B* **1992**, 46, 7185-7188 and Charlier, J.-C.; Gonze, X.; Michenaud, J.-P. *Carbon* **1994**, 32, 289-299.

50 Donchev, A. G. *Phys. Rev. B* **2006**, 74, 235401 1-6. For some pertinent comments on exfoliation and cohesion energies, see in particular its Introduction and its note 39. Actually, as remarked by Donchev, the value put forward by Zacharia, Ulbricht, and Hertel in ref. 30 is "a theoretical prediction, based on a force field … fitted to the actual experimental data on PAH-graphite binding energies".

51 Hasegawa, M.; Nishidate, K. *Phys. Rev. B* **2004**, 70, 205431 1-7.

52 Girifalco, L. A.; Lad, R. A. *J. Chem. Phys.* **1956**, 25, 693-697.

53 Guilloteau, A.; Bedjanian, Y.; Nguyen, M. L. ; Tomas, A. *J. Phys. Chem. A* **2010**, 114, 942-948.

54 Bedjanian, Y.; Nguyen, M. L.; Guilloteau, A. *J. Phys. Chem. A* **2010**, 114, 3533–3539.

55 Glassman, I.; Yetter, R. A. *Combustion*. Academic Press (Elsevier), 2008. See ch. 8, Table 8.6, p. 467.

56 Sirignano, M.; Kent, J.; D'Anna, A. *Comb. Flame* **2010**, 157, 1211–1219.

57 Compare for instance the discussion in: Wang, Q. *Phys. Lett. A* **2010**, 374, 1180–1183, where the *flexural rigidity* is found to be dependent on the size and the shape of graphene sheets.

58 Graphene sheets have been recently shown to be even capable of folding, suggesting that the conjugated π network is capable of extremely sharp curvature: Allen, M. J.; Wang, M.; Jannuzzi, S. A. V.; Yang, Y.; Wang, K. L.; Kaner, R. B. *Chem. Commun*. **2009**, 41, 6285–6287.

59 Palser, A. H. *Phys. Chem. Chem. Phys*. **1999**, 1, 4459-4464. The flexibility of a graphenic structure is suggested by the very existence of nanotubes.

60 The electrostatic contribution depends on the electronegativity χ of carbon, which depends in turn on its hybridation. Since C(sp) in ethyne has more s character than C(sp^2) in ethene, this empirical quantity is consequently estimated to be larger for carbon in the former: χ= 3.29 for the sp hybridation, and χ= 2.75 for the sp^2 (for sp^3, χ= 2.5). Thus, the interaction involving one ethyne C–H bond and a site offering some electron density (as a π system of an aromatic ring) more closely resembles a hydrogen bond. The χ values parallel the estimated pK_a values for alkynes and alkenes which provide a measure of the stability of the corresponding carbanion (ethyne: pK_a =25, ethene pK_a =44; from Smith, M. B.; March, J. *March's Advanced Organic Chemistry*, Wiley, 2001, ch. 8, Table 8.1).